CONJUGATED HEAT TRANSFER MODELS FOR HEATED AERONAUTICAL PITOT TUBES: EXPERIMENTAL VALIDATION WITH A4 SKYHAWK FLIGHT TESTS

José Roberto Brito de Souza, jr.bs1959@gmail.com
Kleber Marques Lisboa, kleberlisboa@poli.ufrj.br
Ivana Gabriela Cerqueira, igabi@ufrj.br
Carolina P. Naveira-Cotta, carolina@mecanica.ufrj.br
Renato M. Cotta, cotta@mecanica.ufrj.br
Laboratório de Transmissão e Tecnologia do Calor – LTTC, POLI & COPPE/UFRJ, Rio de Janeiro, RJ
José Luiz Zanon Zotin, jlzzotin@gmail.com
INMETRO, Rio de Janeiro, RJ

Abstract. *The purpose of this work is to study both theoretically and experimentally the conjugated heat transfer problem associated with the transient thermal behavior of a heated aeronautical Pitot tube, here illustrated by the aircraft A4 Skyhawk probe of the Brazilian Navy. The aim is to demonstrate the importance of accounting for the conduction-convection conjugation in more complex models that attempt to predict the icing of such sensors under severe atmospheric conditions. The experimental analysis involves the use of thermocouples fixed to the surface of the Pitot tube and temperature measurements acquired by a data logger installed in the frontal cone of the airplane. The theoretical analysis involves the proposition of an improved lumped-differential model for heat conduction along the probe, approximating the transversal temperature gradients within the metallic and ceramic walls. The convective heat transfer problem in the fluid is solved using the boundary layer equations for compressible flow, applying the Illingsworth variables transformation considering a locally similar flow. The nonlinear partial differential equations are solved using the Generalized Integral Transform Technique (GITT) in the Mathematica v7.0 platform.*

Keywords: *conjugated problem, compressible flow, anti-icing, lumped analysis, Pitot tube, boundary layer equations*

1. INTRODUCTION

Icing is well known for being a considerably negative effect on aircraft flight performance. It may occur on wings, control surfaces, horizontal and vertical stabilizers, fuselage nose, landing gear doors, engine intakes, Pitot tubes, and other sensors and drain system outputs (Gent et al., 2000; Caliskan et al., 2008). For instance, icing of the Pitot tube reduces ram air pressure on the airspeed indicator and renders the instrument unreliable. Furthermore, this phenomenon has resulted in several incidents and fatal accidents, such as the recent tragedy with the AF447 flight. While the literature is quite rich in terms of icing and de-icing of wings and engine intakes, reporting in recent works a few different computer codes, such as the well-known LEWICE, ONERA2D and TRAJICE2 for icing of airfoils (Silva et al., 2007; Stefanini et al., 2008), only qualitative information has been published in terms of ice accretion over aircraft Pitot probes.

Conjugated conduction-convection problems are among the few classical formulations in heat transfer that still demand exact analytical treatment. Since the pioneering works of (Perelman, 1961) and (Luikov et al., 1971), such class of problems continuously deserved the attention of various researchers towards the development of approximate solutions, either in external or internal flow situations. For instance, the Generalized Integral Transform Technique, which is the approach here adopted, has been applied itself to obtain hybrid solutions for conjugated conduction-convection problems (Guedes & Cotta, 1992; Naveira et al., 2009; Nunes et al., 2010; Naveira-Cotta et al., 2010), in both steady and transient formulations, by employing a transversally lumped heat conduction equation for the wall temperature.

The present work is thus an extension of previous conjugated conduction-convection analysis, here addressing heated Pitot tubes within a compressible fluid flow and undergoing thermal transients. An improved-lumped-differential model (Cotta & Mikhailov, 1997) is developed to predict temperature distributions along a typical aeronautical Pitot probe. The laminar portion of the flow is modeled through the boundary layer equations using the Illingsworth transformation (White, 1992). For the wing-like part of the sensor a recently published correlation (Tong, 2009) is employed for the calculation of the mean Nusselt number. Correlations are also applied at the stagnation point and at the turbulent portion of the flow. Finally, the partial differential formulations in the solid and fluid regions are numerically integrated using an iterative procedure, which is started by solving the flow for an arbitrary constant wall temperature and then using the resulting Nusselt number distribution to solve the wall heat conduction problem, which provides the feedback for the flow simulation. This operation is repeated until the maximum absolute difference between two consecutive temperature values satisfy a certain convergence criterion. The theoretical predictions are then critically compared to flight tests achieved on the A4 Skyhawk aircraft of the Brazilian Navy, through temperature measurements obtained with thermocouples installed on the Pitot tube external surface, registering the thermal response

to the heat generation transients promoted by the aircraft pilot. Then, critical comparisons of the classical lumping approach and the improved lumped-differential formulation for heat conduction within the probe are provided. Finally, the effect of neglecting the thermal capacitance influence along the probe length is more closely discussed.

2. PHYSICAL AND MATHEMATICAL MODEL

The Pitot tube employed in the analysis here performed is shown in Figures 1, where Fig.1.a shows the graphite ink painted probe as prepared for infrared thermography in the wind tunnel testing, while Fig.1.b illustrates its technical drawings that provided the relevant dimensions for simulation purposes. The analysis of the sensor structure heating and its interaction with the external environment under compressible flow can be a fairly complicated problem, depending on the adopted model. The present work attempts to demonstrate that relatively simple one-dimensional transient models for the probe heat conduction problem and two-dimensional boundary layer models for the heat convection problem can adequately simulate the thermal behavior of this conjugated heat transfer situation. For the purpose of designing or analyzing the anti-icing heating system, attention should be focused on the precise representation of the heat transfer phenomena in the vicinity of the probe´s tip, since icing is known to occur mainly at the stagnation flow region. Therefore, a detailed local reproduction of the temperature field at the wing shaped support of the probe is not so relevant, which allows simplification of the curvature effects in the transition from the conical-cylindrical portion towards the junction with the support, as will be seen in what follows.

Figure 1.a. A4 Skyhawk Pitot tube, manufactured by AeroInstruments Co., USA.

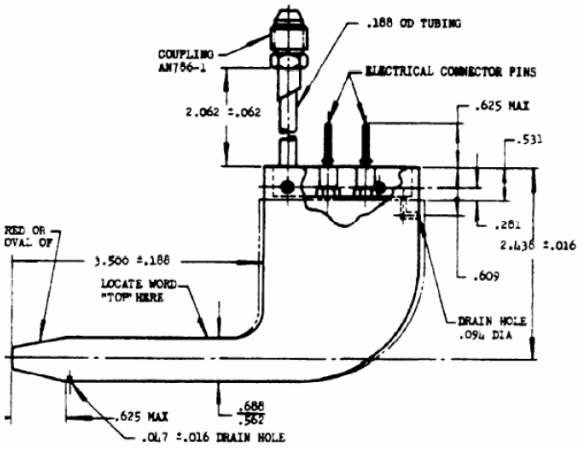

Figure 1.b. Technical drawing of the Pitot tube (source: AeroInstruments Co., USA).

The heat conduction problem for the probe structure is initially based on the transient two-dimensional axisymmetric heat conduction equation in cylindrical coordinates (Souza et al., 2011). It is then simplified resulting in an improved lumped-differential model by using the Coupled Integral Equations Approach (CIEA), revised in (Cotta & Mikhailov, 1997), which approximates the radial temperature gradients across the Pitot tube metalic and ceramic wall, defining a radially averaged temperature and integrating the associated energy equation. This reformulation of the heat conduction problem along the probe length, in dimensionless form, is given by the transient one-dimensional model below:

$$C_t^*(X)\frac{\partial \theta_{av}}{\partial \tau} = \frac{1}{A(X)}\frac{\partial}{\partial X}\left(k^*(X)A(X)\frac{\partial \theta_{av}}{\partial X}\right) - \frac{\Omega(X,\tau)L^2}{k_0}\theta_{av}(X,\tau) + \frac{g_{av}(X,\tau)L^2}{k_0(T_r - T_{aw})} \quad (1.a)$$

where:

$$\Omega(X,\tau) = \frac{24h(X,\tau)R(x)k_s(x)}{(R(X)-R_0(X))[h(X,\tau)(R(X)-R_0(X))(3R(X)+5R_0(X))+12(R(X)+R_0(X))k_s(X)]};\ C_t^*(X) = \frac{\rho_s(X)c_{p_s}(X)}{\rho_0 c_{p_0}};\ k^*(X) = \frac{k_s(X)}{k_0} \quad (1.b\text{-}d)$$

with initial and boundary conditions given by:

$$\theta_{av}(X,0) = \frac{T_0(X)-T_{aw}}{T_r-T_{aw}}, 0 \le X \le 1 \quad (1.e)$$

$$Bi_{e,L}\theta_{av}(0,\tau) - k^*(0)\left.\frac{\partial \theta_{av}}{\partial X}\right|_{X=0} = 0; \qquad Bi_L\theta_{av}(1,\tau) + k^*(1)\left.\frac{\partial \theta_{av}}{\partial X}\right|_{X=1} = 0, \tau > 0 \quad (1.f,g)$$

where the variables correspond to: X, dimensionless longitudinal coordinate, L, length of the Pitot tube [m], τ, dimensionless time, R(X), external radius of the probe [m], R_0(X), internal radius of the probe [m], A(X), probe´s cross section area [m²], θ_{av}(X,τ), dimensionless transversally averaged temperature, g_{av}(X,τ), transversally averaged volumetri heat generation rate [W/m³], h(X,τ), heat transfer coefficient [W/(m²K)], T_r, reference temperature [K], T_{aw}, adiabatic wall temperature [K], ρ_s(X), density of the probe material [kg/m³], c_{ps}(X), specific heat of the probe material [J/(kgK)],

$k_s(X)$, thermal conductivity of the probe material [W/(mK)], ρ_0, reference density [kg/m³], c_{p0}, reference specific heat [J/(kgK)], k_0, reference thermal conductivity [W/(mK)], $Bi_{e,L}$, Biot number at the stagnation point based on the length of the Pitot tube, Bi_L, Biot number at the end based on the length of the Pitot tube.

The boundary layer equations for compressible flow are considered so as to model the laminar flow along the Pitot tube up to the onset of the turbulence transition region. The Illingsworth transformation (White, 1992) is used in order to transform the domain of integration and accelerate the convergence of the solution methodology here implemented. Also, the flow problem is considered to be in quasi-steady state. This has been recently shown to be a quite reasonable hypothesis (Lisboa et al., 2012), since the flow transients caused by the heat generation variations are far more rapid in comparison to the transients that result from the energy balance within the solid. This was also corroborated by the results in (Souza et. al., 2011), in which the use of steady state based correlations resulted in quite good adherence to the experimental data. The transformation relations and the resulting momentum and energy equations are then given by:

$$\xi(x) = \int_0^x \rho_e u_e \mu_e R^2 dx\,, \eta(x,y) = \frac{u_e R}{\sqrt{2\xi}} \int_0^y \rho dy'\,, \frac{u}{u_e} = \frac{\partial f(\xi,\eta)}{\partial \eta}, \Gamma(\xi,\eta) = \frac{T}{T_e} \tag{2.a-d}$$

$$\frac{2\xi}{u_e}\frac{\partial u_e}{\partial \xi}\left(\Gamma - \left(\frac{\partial f}{\partial \eta}\right)^2\right) + f\frac{\partial^2 f}{\partial \eta^2} + \frac{\partial}{\partial \eta}\left(\Gamma^{-1/3}\frac{\partial^2 f}{\partial \eta^2}\right) = 0 \tag{3.a}$$

$$2\xi\frac{\partial f}{\partial \eta}\left(\frac{\Gamma}{T_e}\frac{\partial T_e}{\partial \xi} + \frac{(\gamma-1){M_e}^2}{u_e}\frac{\partial u_e}{\partial \xi}\right) = \frac{1}{Pr}\frac{\partial}{\partial \eta}\left(\Gamma^{-1/3}\frac{\partial \Gamma}{\partial \eta}\right) + f\frac{\partial \Gamma}{\partial \eta} + (\gamma-1){M_e}^2\Gamma^{-1/3}\left(\frac{\partial^2 f}{\partial \eta^2}\right)^2 \tag{3.b}$$

with boundary conditions given by:

$$f(0,\eta) = 1, \Gamma(0,\eta) = 1, \eta > 0 \tag{3.c,d}$$

$$f(\xi,0) = 0,\ f'(\xi,0) = 0,\ f'(\xi,\infty) = 1,\ \Gamma(\xi,0) = \frac{T_{av}}{T_e},\ \Gamma(\xi,\infty) = 1, \xi > 0 \tag{3.e-i}$$

where the variables shown above correspond to x, longitudinal coordinate [m], y, coordinate normal to the surface of the Pitot tube [m], ρ_e, density of the air outside the boundary layer [kg/m³], u_e, fluid velocity outside the boundary layer [m/s], μ_e, dynamic viscosity outside the boundary layer [Pa*s], T_e, fluid temperature outside the boundary layer [K], M_e, Mach number outside the boundary layer, u, flow velocity within the boundary layer [m/s], T, flow temperature within the boundary layer [K], ρ, density of the air in the boundary layer [kg/m³], Pr, Prandtl number, γ, isentropic coefficient, T_{av}, transversally averaged wall temperature [K].

Due to the high velocities involved in the present work, the flow becomes turbulent along the length of the Pitot probe, but sufficiently away from the critical icing region. Thus, a detailed modeling of the turbulence effects are not essential at the present stage of development and, instead, empirical correlations were used for the heat transfer coefficient after the transition point . The transition between laminar and turbulent flow is assumed to abruptly occur at the critical Reynolds number based on the horizontal distance to the stagnation point equal to a prescribed value.

3. SOLUTION METHODOLOGY

To solve the problems stated in section 2, the Generalized Integral Transform Technique (GITT) (Cotta, 1993) is applied with the aid of the numeric-symbolic platform *Mathematica v7.0* (Wolfram, 2005). A sufficiently general one-dimensional problem encompassing the above formulations is shown below:

$$w_m(x)\frac{\partial P_m}{\partial t} = G\big(x,t,P_l(x,t)\big), x_0 \le x \le x_1, t > 0,\ m,l = 1,2,\dots,M \tag{4.a}$$

$$P_m(x,0) = P_{m_0}(x) \tag{4.b}$$

$$\alpha_{0_m} P_m(x_0,t) - \beta_{0_m} K_m(x_0)\frac{\partial P_m}{\partial x}\Big|_{x=x_0} = \phi_{0_m}, \alpha_{1_m} P_m(x_1,t) + \beta_{1_m} K_m(x_1)\frac{\partial P_m}{\partial x}\Big|_{x=x_1} = \phi_{1_m} \tag{4.c,d}$$

In order to solve eqs.(4), one must choose an appropriate eigenvalue problem for the proposition of an eigenfunction expansion. Usually this auxiliary problem can be written in the form of a Sturm-Liouville problem, such as the one presented in eqs. (5.a-c):

$$\frac{d}{dx}\left(K_m(x)\frac{d\psi_{m_i}}{dx}\right) + \left(w_m(x){\mu_{m_i}}^2 - d_m(x)\right)\psi_{m_i}(x) = 0 \tag{5.a}$$

$$\alpha_{0_m}\psi_{m_i}(x_0) - \beta_{0_m}K_m(x_0)\frac{\partial \psi_{m_i}}{\partial x}\Big|_{x=x_0} = 0,\ \alpha_{1_m}\psi_{m_i}(x_1) + \beta_{1_m}K_m(x_1)\frac{\partial \psi_{m_i}}{\partial x}\Big|_{x=x_1} = 0 \tag{5.b,c}$$

Before the integral transformation process, a simple analytical filtering solution ($P=P_f+P^*$) is proposed so as to make the boundary conditions (4.c,d) homogeneous, thus matching the boundary conditions of the eigenvalue problem. The integral transform pair is then proposed, featuring the expressions for the transformed potentials and the inverses:

$$\bar{P}_{m_i}(t) = \int_{x_0}^{x_1} w(x)\psi_{m_i}(x){P^*}_m(x,t)dx\,,\quad {P^*}_m(x,t) = \sum_{i=1}^{\infty}\psi_{m_i}(x)\bar{P}_{m_i}(t)\,,\ \text{transform and inverse formulae} \tag{6.a,b}$$

Finally, the integral transform is applied to equation (4.a) and to its initial condition, making use of the eigenfunctions' orthogonality property along with the inversion formula for the filtered potentials eq. (6.b), to obtain the set of transformed ordinary differential equations shown below:

$$\frac{d\bar{P}_{m_i}}{dt} = \int_{x_0}^{x_1} w(x)\,\psi_{m_i}(x) G\big(x,t,P_l(x,t)\big)dx, i = 1,2,\dots,N, m, l = 1,2,\dots,M \tag{7.a}$$

$$\bar{P}_{m_i}(0) = \int_{x_0}^{x_1} w(x)\,\psi_{m_i}(x)\left(P_{m_0}(x) - F_m(x)\right)dx \tag{7.b}$$

The above initial value problems are then solved using the implicit backward differentiation formulas (BDF) method which is built-in the software *Mathematica v7.0* (Wolfram, 2005). A good strategy for accelerating the convergence of the GITT method is to use an auxiliary eigenvalue problem as close as possible to the original problem being solved. However, in many situations a closed form analytical solution to the most adequate auxiliary problems are not readily available. In such cases, it is recommended that the eigenvalue problem itself should be solved by the GITT. The basic idea in this approach is to propose a simpler eigenvalue problem to serve as a basis for the expansion of the original eigenfunction that represents more adequately the problem under consideration. For instance, in solving the heat conduction problem along the Pitot tube, the following eigenvalue problem is suggested:

$$\frac{d}{dX}\left(k^*(X)A(X)\frac{d\varphi_i}{dX}\right) + {C_t}^*(X)A(X){\lambda_i}^2\varphi_i = 0 \tag{8}$$

with the appropriate boundary conditions corresponding to eqs.(1.f,g).

Although there exist routines capable of solving boundary value problems such as the ones involved in the flow problem in a satisfactory manner, the robustness is still not as good as that of the algorithms developed for solving initial value problems. In this particular case, none of the algorithms for solving boundary value problems implemented in the software *Mathematica* 7.0 (Wolfram, 2005) were capable of solving the equations considering the variation of the thermophysical properties with temperature. In order to avoid such difficulties, a pseudo-transient formulation is here employed to solve the compressible boundary layer equations using the GITT (Cotta, 1993). Also, the flow boundary layer equation as presented in equation (3.a) consists of a third order differential equation, but after eqs. (11.a,b) below are substituted into eqs. (3.a-i), it becomes a second order equation, but with the expense that both equations are now integro-differential equations.

$$f(\xi,\eta) = \int_0^\eta \zeta(\xi,\eta^*)d\eta^*, \quad \zeta(\xi,\eta) = \frac{\partial f}{\partial \eta} \tag{11.a,b}$$

Nevertheless, this does not pose any difficulty to application of the integral transform method, and allows for a more clear identification of the adequate eigenvalue problem from the second order operators. Using the assumption of locally similar flow, the equations are solved for 15 different stations along the Pitot tube, with the final point being that of the abrupt transition to turbulent flow. The heat transfer coefficient present in equation (1.b) is responsible for the coupling between the heat transfer models in the solid and in the fluid. The governing equations are then solved in an iterative procedure similar to that implemented in (Lisboa et. al., 2012). First, the boundary layer equations are solved for an arbitrary uniform wall temperature. The heat transfer coefficient is then calculated, generating the results of the temperature field in the solid. This steady-state temperature field is then fed back into the flow equations. This is done until the maximum difference between two consecutive temperature fields satisfies an user prescribed convergence criteria.

4. A4 SKYHAWK FLIGHT TESTS

The experimental results for the transient thermal behavior of the heated Pitot tube were obtained on an A4-Skyhawk airplane of the VF-1 Squadron, in the Brazilian Aero-Naval Base, at São Pedro d´Aldeia, Rio de Janeiro, shown in Figs. 2.a-b below. The A4 is a single seat, light weight, high performance attack aircraft with a modified delta planform wing. It was designed for strike, interdiction, close support and training. It is powered by a Pratt & Whitney gas turbine engine that produces a sea level static thrust of 11,200 pounds, making it possible to the aircraft to reach transonic speeds. The main components of this experimental campaign are the A-4 Pitot tube and the TESTO Data Logger, model 177-T4. The data logger has four temperature channels which were used during the test flight, with type K thermocouples in a measuring rate of 3 s, and was switched on still on the ground, before the pilot powered the plane. The data logger was positioned in the front compartment of the plane, and fixed with plastic tape in a thermally insulated box, Fig. 2.c. The thermocouples were fixed at increasing longitudinal distances from the tip of the Pitot tube (Fig.2.d), by a special glue made by Loctite, E-20NS Hysol Epoxy Adhesive, which is a long time curing, low viscosity structural adhesive.

After takeoff, two thermocouples were damaged, numbers 1 and 2, when the temperature of the wall of the Pitot sensor reached temperatures over 270 °C followed by the airplane acceleration. Thus, during the flight, only the

temperatures from the thermocouples numbers 3 and 4 were recorded. Thermocouple number 3 was attached approximately at the end of the heated portion of the cylindrical body of the Pitot probe (x=80 mm). Thermocouple number 4 was attached to the wing-shaped base of the Pitot probe, and its sensing tip was exposed to measure the external atmospheric temperature. The pilot was then responsible for promoting a transient thermal behavior on the Pitot tube, by turning it off for a few seconds and then on again, at different stable planned altitudes.

Figure 2.a. A4 Skyhawk airplane with tested Pitot probe.

Figure 2.b. Installation of the Pitot tube on the aircraft.

Figure 2.c. Insulated data logger in the front compartment.

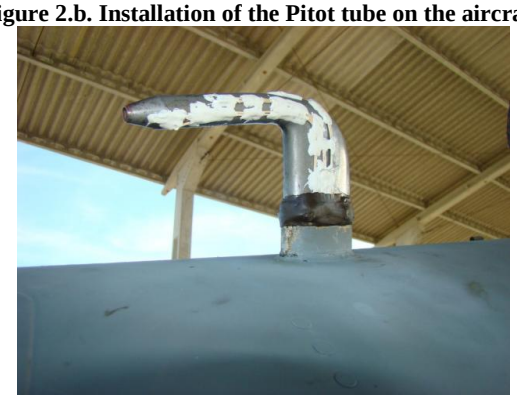

Figure 2.d. Detail of the thermocouples positioning.

5. RESULTS AND DISCUSSION

Before proceeding to the comparison of the flight test results against the proposed simulation, the model was validated against more controlled experimental results previously obtained in (Souza et. al., 2011). In that paper, an experimental investigation was performed at the wind tunnel facilities of the National Institute of Metrology, Standardization and Industrial Quality (INMETRO), in the subsonic regime, and transient temperature distributions were obtained with an infrared camera thermography. The experimental results then obtained are here compared with the simulation performed using CIEA/GITT and the iterative procedure described in section 3. Figure 3 illustrates the comparison of the steady state temperature distribution along the Pitot probe surface. Clearly, a good agreement was achieved between the theoretical and experimental curves, giving confidence on the model and on the constructed solver, which were shown to be indeed effective. Another result of interest is the distribution of the local heat transfer coefficient along the length of the Pitot probe, for the wind tunnel experimental conditions, which is shown in Fig. 4. This curve illustrates the different heat transfer coefficient behaviors in the regions along the Pitot corresponding to the stagnation point, conical section, cylindrical body (laminar flow only) and the average coefficient at the support.

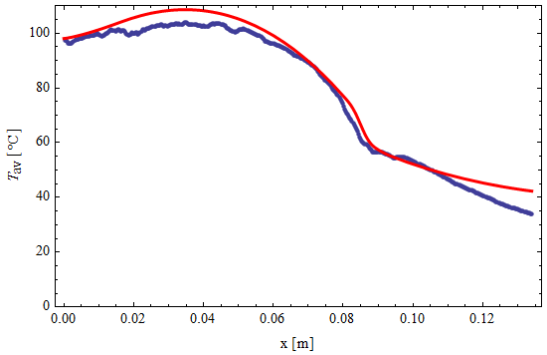

Figure 3. Comparison of experimental (blue) and theoretical (red) steady temperatures along the probe (u_∞=10m/s).

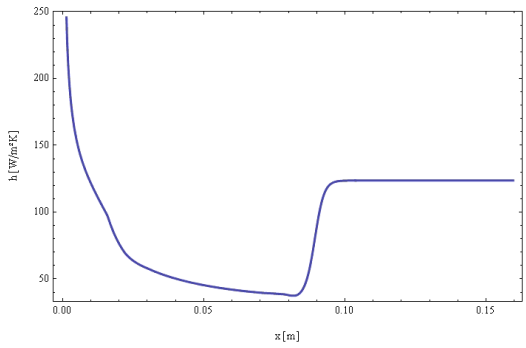

Figure 4. Heat transfer coefficient along the Pitot length for the wind tunnel test conditions.

The convergence of the iterative procedure in the solution of the conjugated heat transfer problem was observed to be quite effective, such as in the previous contribution (Lisboa et al., 2012). The residue of the dimensionless temperatures was controlled to within the accuracy of 10^{-5}, and convergence was achieved with only 5 iterations for the 10000 ft case and with 6 iterations for the 15000 ft run. Another interesting methodology aspect is the convergence of the Generalized Integral Transform Technique (GITT) with respect to the truncation order of the eigenfunctions expansion. Tables 1 and 2 illustrate the convergence for the dimensionless solid temperature and for the dimensionless flow velocity distribution (x=11mm), respectively, at t=476 s for the case at an altitude of 10000 ft. Convergence to the fourth significant digit is achieved in all cases illustrated, with the flow problem requiring lower truncation orders for convergence than the probe heat conduction problem.

Table 1. Convergence analysis of the dimensionless average probe temperature at an altitude of 10000 ft.

	X=0.	X=0.1	X=0.2	X=0.3	X=0.4	X=0.5	X=0.6	X=0.7	X=0.8	X=0.9	X=1.
N=5	-1.37529	-1.39695	-1.48537	-1.53114	-1.32807	-0.844258	-0.319164	-0.176786	-0.106822	-0.0725297	-0.0603954
N=10	-1.26548	-1.35974	-1.53757	-1.49274	-1.33467	-0.86164	-0.311541	-0.179329	-0.108789	-0.070499	-0.0614238
N=15	-1.19264	-1.3731	-1.51789	-1.50802	-1.32334	-0.873563	-0.308035	-0.180358	-0.108962	-0.0714522	-0.0594664
N=20	-1.18651	-1.37702	-1.51929	-1.50645	-1.32199	-0.874904	-0.309895	-0.180305	-0.107931	-0.0715785	-0.0605698
N=25	-1.18841	-1.37622	-1.51939	-1.50681	-1.3221	-0.875295	-0.310285	-0.180382	-0.107666	-0.0714291	-0.0606023
N=30	-1.19087	-1.37635	-1.51977	-1.50651	-1.322	-0.875712	-0.310195	-0.180229	-0.107832	-0.071462	-0.060443
N=35	-1.19056	-1.37617	-1.51981	-1.5066	-1.32207	-0.875638	-0.310135	-0.180286	-0.107853	-0.0714447	-0.0604091
N=40	-1.1879	-1.37599	-1.51959	-1.50648	-1.32206	-0.875666	-0.310123	-0.180241	-0.107818	-0.071451	-0.0604388

Table 2. Convergence of the dimensionless flow velocity distribution at x=11 mm from the stagnation point at an altitude of 10000 ft.

	η=0.	η=0.6	η=1.2	η=1.8	η=2.4	η=3.	η=3.6	η=4.2	η=4.8	η=5.4	η=6.
N=5	0	0.35357	0.643145	0.836952	0.941641	0.985201	0.997361	0.999081	0.99981	1.00045	1.
N=10	0	0.355541	0.641069	0.837544	0.942237	0.98483	0.9969	0.999649	0.999901	1.00001	1.
N=15	0	0.355034	0.641591	0.837298	0.942372	0.984644	0.997043	0.999615	0.999932	0.999944	1.
N=20	0	0.354857	0.6414	0.837234	0.94241	0.984664	0.996995	0.999565	0.999945	0.999988	1.

Next, the A4 flight tests results are compared to the proposed theoretical model, for two sample runs at altitudes of 10000 ft (3048 m) and 15000 ft (4572 m) with Mach numbers of 0.5 (591.1 km/h) and 0.51 (591.7 km/h), respectively. Two different results for each of the flight conditions are presented below in Figures 5.a,b and 6.a,b, respectively, in which the difference between graphs a and b stands for accounting or not accounting for the considerable thermal capacitance of the porcelain electrical insulator within the Pitot probe body. In order to illustrate the significance of the conjugated heat transfer problem in the adequate safety analysis of such class of sensors when subjected to severe transients, we compare the experimental and theoretical results for the Pitot probe surface temperature (x=80 mm) first by considering the insulator, in Figures 5.a and 6.a, with excellent agreement throughout the pilot promoted transients. On the other hand, when the insulator is disregarded, in Figures 5.b and 6.b, the simulations significantly underestimate the required time for thermal recovery of the probe after being subjected to a shutdown and startup sequence, with the experiments being much slower than the simulations.

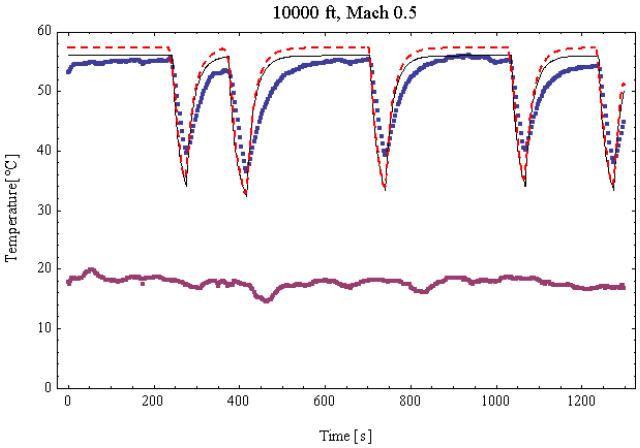

Figure 5.a. Comparison of A4 test experimental (blue dots) and theoretical (CIEA: black line; Classical Lumping: dashed red line) temperature transients (x=80mm), accounting for thermal capacitance of porcelain insulator.

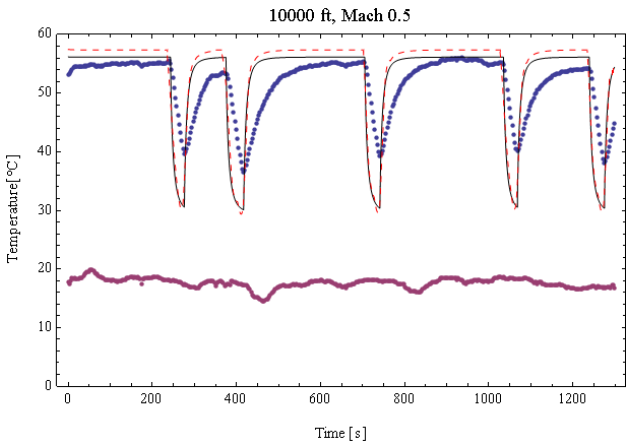

Figure 5.b. Comparison of A4 test experimental (blue dots) and theoretical (CIEA: black line; Classical Lumping: dashed red line) temperature transients (x=80mm), not accounting for porcelain insulator participation.

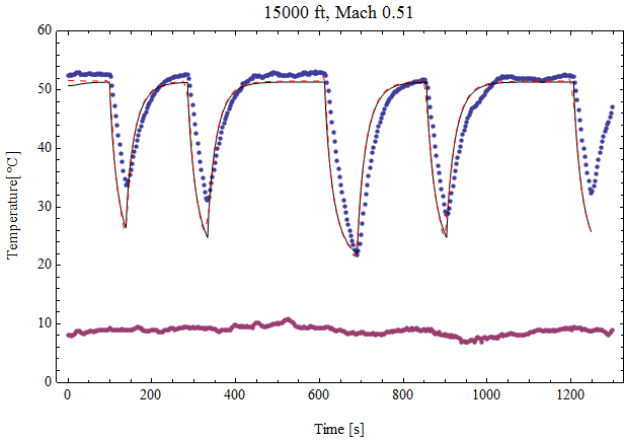

Figure 6.a. Comparison of A4 test experimental (blue dots) and theoretical (CIEA: black line; Classical Lumping: dashed red line) temperature transients (x=80mm), accounting for thermal capacitance of porcelain insulator.

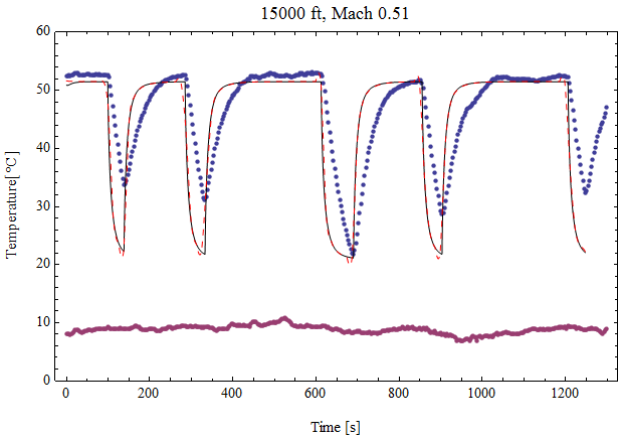

Figure 6.b. Comparison of A4 test experimental (blue dots) and theoretical (CIEA: black line; Classical Lumping: dashed red line) temperature transients (x=80mm), not accounting for porcelain insulator participation.

Figures 7.a and 8.a present the theoretical prediction of the steady-state results along the probe length, for the two altitudes (10.000 and 15.000 ft), respectively, while Figures 7.b and 8.b illustrate the spatial behavior of the heat transfer coefficient for the two situations. It can be observed that temperature distributions follow the expected behavior observed in the controlled wind tunnel experiment, showing that the maximum temperatures are achieved within the heated portion in the cylindrical section, and a significant temperature drop is observed at the probe tip, which is the critical region in the design of the anti-icing system. Another aspect worth mentioning, form Figs.7.b and 8.b is the presence of the turbulent region in these cases, which significantly modifies the heat transfer coefficient distribution in comparison to the low speed experiments in the wind tunnel as shown in Fig. 4. Also it is noticeable that the heat transfer coefficients calculated for the 15000 ft run are considerably lower than those for the 10000 ft experiment. The lower values of the heat transfer coefficient yield lower values of the Biot numbers, which then favor the accuracy of the lumping procedures. This behavior explains the better agreement of the classical (dashed red line) and improved (black line) lumping approaches for the case of 15000ft, as observed in Fig. 6.a, while for the run at 10000ft, with higher heat transfer coefficients, Fig.5.a, an average deviation of around 3% is observed between the two models.

In conclusion, the main objective of the present work was achieved with respect to the construction of a fairly simple model for the conjugated heat transfer analysis in heated Pitot probes, subjected to forced transient loads or time variable external conditions in actual flight conditions. The model here validated by the A4 flight experimental data, may already be employed in the analysis of more severe conditions, in the design and optimization of anti-icing systems, and as the basic heat transfer formulation for the incorporation of icing accretion models. It is also possible to make use of this model to do preliminary analysis with different geometries in order to observe their influence in the temperature distribution, most especially at the stagnation point vicinity that is critical for the reliability of the sensor within icing environment.

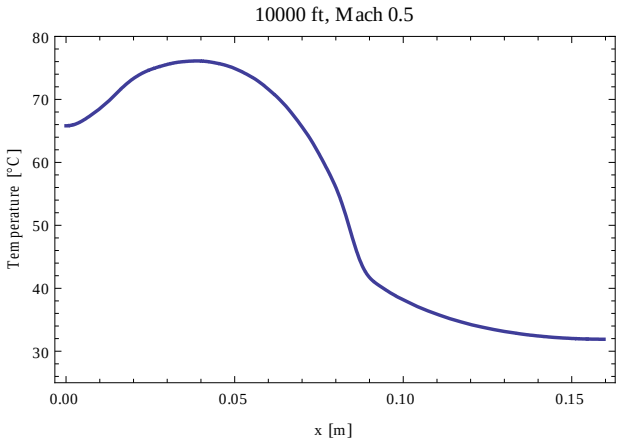

Figure 7.a. Steady-state temperature distribution along the Pitot tube (10000 ft).

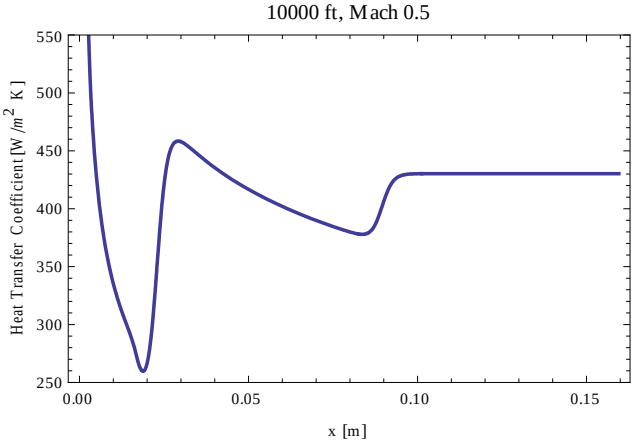

Figure 7.b. Local heat transfer coefficient along the Pitot tube(10000 ft).

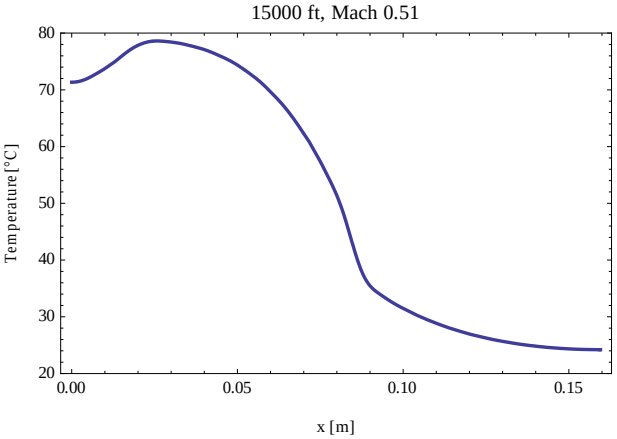

Figure 8.a. Steady-state temperature distribution along the Pitot tube (15000 ft).

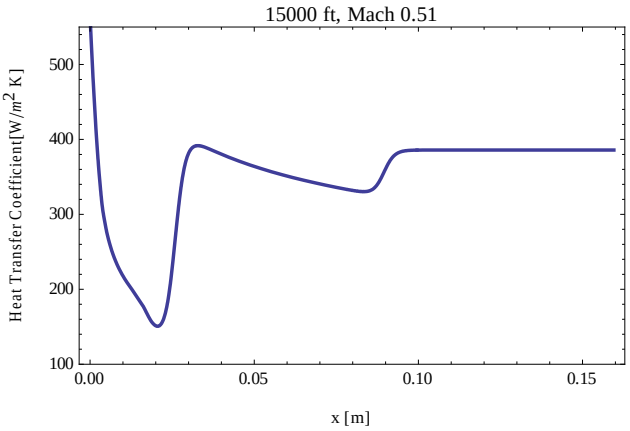

Figure 8.b. Local heat transfer coefficient along the Pitot tube(15000 ft).

6. ACKNOWLEDGEMENTS

The authors are indebted to the Brazilian Navy, for providing the Pitot tubes here employed and sponsoring the A4 flight tests. The financial support of CNPq and FAPERJ is also acknowledged. This work is dedicated to the 228 victims of the AF447 flight and their families, hoping that such hard lessons will affect somehow technology development protocols in a progressively more competitive world, by strictly bounding them with scientific analysis.

7. REFERENCES

Caliskan; F., Aykan, R., and Hajiyev, C., 2008, Aircraft Icing Detection, Identification, and Reconfigurable Control Based on Kalman Filtering and Neural Networks, J. of Aerospace Engineering, v. 21, no. 2, pp.51-60.

Cotta, R.M. , 1993, Integral Transforms in Computational Heat and Fluid Flow, CRC Press, Boca Raton.

Cotta, R.M. and Mikhailov, M.D., 1997, Heat Conduction: Lumped Analysis, Integral Transforms, Symbolic Computation, Wiley-Interscience, Chichester, UK.

Guedes, R.O.C. and Cotta, R.M., 1991, Periodic Laminar Forced Convection within Ducts Including Wall Heat Conduction Effects, Int. J. Eng. Sci, Vol. 29, No.5, pp. 535-547.

Gent, R. W., Dart, N. P., and Cansdale, J. T., 2000, Aircraft Icing, Phil. Trans. R. Soc. Lond. A, v. 358, pp.2873-2911.

Lisboa, K.M., Souza, J.R.B., Cotta, R.M., Naveira-Cotta, C.P., 2012, Transient Conjugated Heat Transfer in External Compressible Laminar Flow over Plates with Internal Heat Generation, Proc. of the 7th CONEM - Congresso Nacional de Engenharia Mecânica, São Luis, MA, Brazil.

Luikov, A.V., Aleksashenko, V.A., and Aleksashenko, A.A., 1971, Analytical Methods of Solution of Conjugated Problems in Convective Heat Transfer, Int. J. Heat and Mass Transfer, Vol. 14, pp. 1047-1056.

Naveira, C.P., Lachi, M., Cotta, R.M., Padet, J., 2009, Hybrid Formulation and Solution for Transient Conjugated Conduction-External Convection, Int. J. Heat & Mass Transfer, Vol. 52, Issues 1-2, pp. 112-123.

Naveira-Cotta, C.P., Lachi, M., Rebay, M., and Cotta, R.M., 2010, Experiments and Simulations in Transient Conjugated Conduction-Convection-Radiation, Heat Transfer Research, Vol.43, No.3, pp. 209-231.

Nunes, J.S., Cotta, R.M., Avelino, M.R., and Kakaç, S., 2010, Conjugated Heat Transfer in Microchannels, NATO Science for Peace and Security Series A: Chemistry and Biology, Microfluidics Based Microsystems: Fundamentals and Applications, Kakaç, S., Kosoy, B., Pramuanjaroenkij, A. (Eds.), pp. 61-82.

Perelman, Y.L., 1961, On Conjugate Problems of Heat Transfer, Int. J. Heat and Mass Transfer, Vol. 3, pp.293-303.

Souza, J.B.R., Zotin, J.L.Z., Loureiro, J.B.R., Naveira-Cotta, C.P., Silva Freire, A.P., and Cotta, R.M., 2011, Conjugated Heat Transfer Analysis of Heated Pitot Tubes: Wind Tunnel Experiments, Infrared Thermography and Lumped-Differential Modeling, 21st COBEM- Congresso Brasileiro de Engenharia Mecânica, 2011, Natal, Brazil.

Sparrow, E.M., Abraham, J.P., Tong, J.C.K., 2004, Archival Correlations for Average Heat Transfer Coefficients for Non-circular and Circular Cylinders and for Spheres in Cross-flow, Int. J. Heat Mass Transfer, v.47, pp.5285-5296.

Silva, G. A. L., Silvares, O. M., and Zerbini, E. J. G. J., 2007, Numerical Simulation of Airfoil Thermal Anti-Ice Operation Part 1: Mathematical Modeling, J. of Aircraft, Vol. 44, No. 2, March–April.

Stefanini, L. M., Silvares, O. M., Silva, G. A. L., and Zerbini, E. J. G. J., 2008, Boundary-Layers Integral Analysis - Airfoil Icing, AIAA Paper 2008-0474, Aerospace Sciences Meeting and Exhibit, 46th, 2008, Reno, American Institute of Aeronautics and Astronautics, Reston.

Tong, Z.M., and Hu, Y.H., 2009, Convective Heat Transfer and Flow Resistance Characteristics of Various Types of Elliptical Tubes, Proc. of the Int. Conf. on Energy and Environment Technology, IEEE.

White F. M., 1992, Viscous Fluid Flow, McGraw-Hill.

Wolfram, S., 2005, The *Mathematica* Book, Cambridge-Wolfram Media.